Disentangling multipole resonances through a full x-ray polarization analysis

C. Mazzoli,[1] S. B. Wilkins,[1,2] S. Di Matteo,[3,4] B. Detlefs,[1,5] C. Detlefs,[1] V. Scagnoli,[1] L. Paolasini,[1] and P. Ghigna[6]

[1]*European Synchrotron Radiation Facility, BP 220, F-38043 Grenoble Cedex 9, France*
[2]*Brookhaven National Laboratory, Condensed Matter Physics & Materials Science Department, Upton, New York, 11973-5000, USA*
[3]*Laboratori Nazionali di Frascati INFN, via E. Fermi 40, C.P. 13, I-00044 Frascati (Roma), Italy*
[4]*Equipe de physique des surfaces et interfaces, UMR-CNRS 6627 PALMS, Université de Rennes 1, 35042 Rennes Cedex, France*
[5]*European Commission, JRC, Institute for Transuranium Elements, Postfach 2340, Karlsruhe, D-76125 Germany*
[6]*Dipartimento di Chimica Fisica "M. Rolla," Universitá di Pavia, I-27100 Pavia, Italy*
(Received 2 July 2007; published 20 November 2007)

Complete polarization analysis applied to resonant x-ray scattering at the Cr K edge in K_2CrO_4 shows that incident linearly polarized x rays can be converted into circularly polarized x rays by diffraction at the Cr pre-edge ($E=5994$ eV). The physical mechanism behind this phenomenon is a subtle interference effect between purely dipole ($E1$-$E1$) and purely quadrupole ($E2$-$E2$) transitions, leading to a phase shift between the respective scattering amplitudes. This effect may be exploited to disentangle two close-lying resonances that appear as a single peak in a conventional energy scan, in this way allowing one to single out and identify the different multipole order parameters involved.

I. INTRODUCTION

In the last 10 years resonant x-ray scattering (RXS) has developed into a powerful technique to obtain direct information about charge, magnetic, and orbital degrees of freedom.[1–6] It combines the high sensitivity of x-ray diffraction to long-range-ordered structures with that of x-ray-absorption spectroscopy to local electronic configurations. In particular, the development of third-generation synchrotron radiation sources has made possible the detection of small effects in electronic distribution, due to magnetoelectric anisotropy[7] or to local chirality,[8,9] which can be related to the interference between dipole ($E1$) and quadrupole ($E2$) resonances. These pioneering studies paved the way to a new interpretation of RXS experiments in terms of electromagnetic multipoles of higher order than dipole and led to the detection of phase transitions characterized by order parameters (OPs) of exotic symmetry.[10–12] Several theories have been developed, based on these higher-order OP, to explain "anomalous" phase transitions. For example, in NpO_2 a proper interpretation of the magnetic ground state requires a primary OP at least octupolar order,[13] whereas in high-temperature cuprate superconductors, the pseudogap phase has been interpreted in terms of parity and time-reversal odd toroidal multipoles.[14,15] In several cases, though, the assignment of the multipolar origin to a RXS signal is not clear.[10,16,17] The characteristic variation of the intensity and polarization as the sample is rotated about the scattering vector during an azimuthal scan may allow a clearer identification of the order of the multipole. However, this technique is plagued by many experimental difficulties either from the sample—e.g., when the crystal presents twinning and mosaicity—or due to restrictive sample environments, such as cryomagnets. Moreover, it is very difficult to identify and resolve two resonances of different multipolar origin when they are separated by less than ∼1eV, a situation which frequently occurs at the metal pre-K-edge region of transition-metal oxides, where $E1$ and $E2$ transitions can have similar

magnitudes, or at $L_{2,3}$ edges of rare-earth compounds. For example, at the Fe pre-K-edge in α-Fe_2O_3, evidence of a $E2$-$E2$ transition was found already in 1993.[18] This transition was interpreted as the signature of a hexadecapolar electronic ordering.[19] Later, however, it was shown by symmetry arguments that also an axial-toroidal-quadrupole OP, parity breaking, was hidden within the same resonance,[11] but to date no conclusive experimental evidence for this interpretation has been provided. Analogously, at the Ce $L_{2,3}$ edges in $CeFe_2$ the different electronic OPs related to $4f$ and $5d$ states are entangled and cannot be examined individually by conventional RXS.[20] A further example is provided by K_2CrO_4. Its space group symmetry ($Pnma$, No. 62) allows several excitation channels at the $(1k0)$ Bragg-forbidden reflections,[21] due to the presence of multipole moments of different symmetries (electric quadrupole, octupole, hexadecapole) in the same energy range, as described in more detail below.

The aim of the present article is to address the previous problems by extending the well-known techniques of optical polarimetry from the visible to the x-ray regime, as developed at the ID20 beamline[22] at the ESRF, Grenoble, France. By using a diamond x-ray phase plate to rotate the incident linear polarization in combination with a linear polarization analyzer, we can resolve resonances determined by multipoles of different order that are very close in energy, playing on their relative phase shifts. The idea can be explained through a simplified model by considering two externally driven, damped harmonic oscillators of unitary amplitude, but with resonant frequencies differing by 2ζ. The scattering amplitude of such oscillators is given by

$$g_\pm(\omega) = \frac{1}{\omega \pm \zeta - i\Gamma}. \quad (1)$$

Here Γ is the inverse damping time and ω the frequency of the external excitation. We also suppose that the two resonances scatter in different polarization channels. Using the

Jones matrix formalism[23] the (unnormalized) polarization of the scattered beam may then be written as $\epsilon' = G\epsilon$, where ϵ (ϵ') are the incident (scattered) polarization vectors and the matrix

$$G = \begin{pmatrix} g_- & g_+ \\ g_+ & g_- \end{pmatrix}$$

contains the dependence on the photon energy. Experimentally, the scattered beam polarization is best described in terms of the Poincaré-Stokes parameters

$$P_1' \equiv \frac{|\epsilon_\sigma'|^2 - |\epsilon_\pi'|^2}{P_0'},$$

$$P_2' \equiv 2\Re e \frac{\epsilon_\sigma'^* \epsilon_\pi'}{P_0'},$$

$$P_3' \equiv 2\Im m \frac{\epsilon_\sigma'^* \epsilon_\pi'}{P_0'},$$

with $P_0' \equiv (|\epsilon_\sigma'|^2 + |\epsilon_\pi'|^2)$ the total intensity and ϵ'^* the complex conjugate of ϵ'. P_1' and P_2' describe the linear polarization states, whereas P_3' indicates the degree of the circular polarization. The Poincaré-Stokes parameters $P_{0,1,2,3}$ of the incident beam are obtained by substituting ϵ for ϵ'.

For example, for an incoming π polarized beam

$$\epsilon = \begin{pmatrix} 0 \\ 1 \end{pmatrix},$$

we obtain

$$\begin{pmatrix} \epsilon_\sigma' \\ \epsilon_\pi' \end{pmatrix} = \begin{pmatrix} g_+ \\ g_- \end{pmatrix},$$

which in turn yields

$$P_1' = -\frac{2\zeta\omega}{\omega^2 + \zeta^2 + \Gamma^2},$$

$$P_2' = +\frac{\omega^2 - \zeta^2 + \Gamma^2}{\omega^2 + \zeta^2 + \Gamma^2},$$

$$P_3' = +\frac{2\zeta\Gamma}{\omega^2 + \zeta^2 + \Gamma^2}. \tag{2}$$

Therefore we expect that in the intermediate region between the two resonances, the outgoing beam is circularly polarized, depending on the relative dephasing of the two resonances, as shown in Fig. 1 for the case $\zeta = \Gamma$.

Below, we describe experimental data which we then compare to quantitative *ab initio* calculations carried out using the FDMNES code.[24] We demonstrate that a 100% linear-to circular-polarization conversion at the pre-edge region of the Cr K edge in K_2CrO_4 is induced by the interference of the dispersive and absorptive parts of two different multipoles probed by purely dipole ($E1$-$E1$) and purely quadrupole ($E2$-$E2$) resonances. Thus, the scattered beam
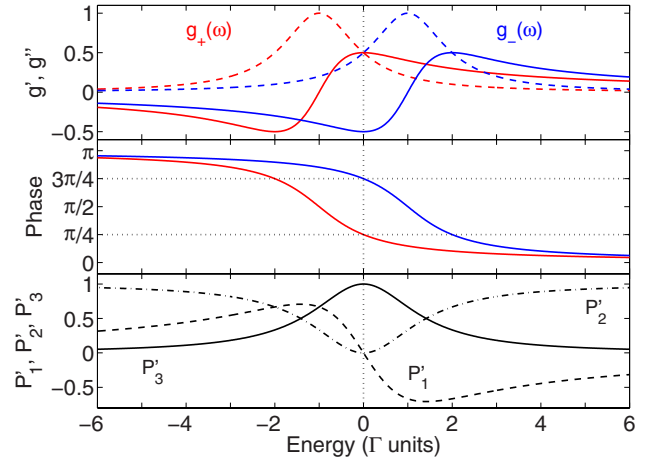

FIG. 1. (Color online) Top: typical behavior of real (g', solid line) and imaginary (g'', dashed line) parts for the two resonators of Eq. (1) (g_+, red; g_-, blue), with $\zeta = \Gamma$. Middle: corresponding phase shifts. Bottom: Poincaré-Stokes parameters as calculated from Eq. (3).

originates from two different excitation channels, each scattering the beam with a different phase.

Their relative amplitudes, at a given energy, are governed by the probed multipoles, the relative orientation of the incident and scattered electric field vectors to the probed multipoles and the reciprocal lattice point under study. Their interference can therefore be tuned simply by varying the incident polarization by means of a phase plate.

II. EXPERIMENTAL SETUP

Experiments were carried out at ID20, ESRF. The experimental setup is outlined in Fig. 2. A single crystal of K_2CrO_4 was mounted on the six-circle horizontal diffractometer, and
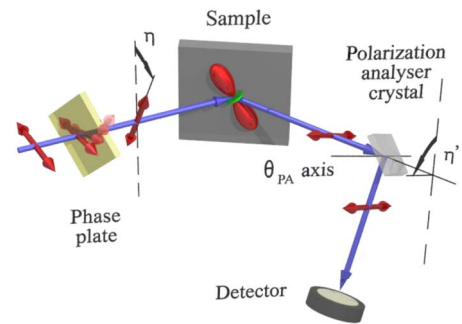

FIG. 2. (Color online) Experimental setup with phase plate in half-wave mode; x-ray directions indicated by blue arrows, polarizations by red ones. Synchrotron light arrives from the left, horizontally polarized (π). η is the rotation angle of the incident polarization. η' is the rotation angle of the polarization analyzer crystal; the zero positions of the two angles, corresponding to σ and σ' polarizations respectively, are represented by dashed lines. The solid line is the rocking axis of the polarization analysis crystal θ_{PA}. The polarization analyzer stage is shown in the configuration corresponding to the maximum detected intensity.
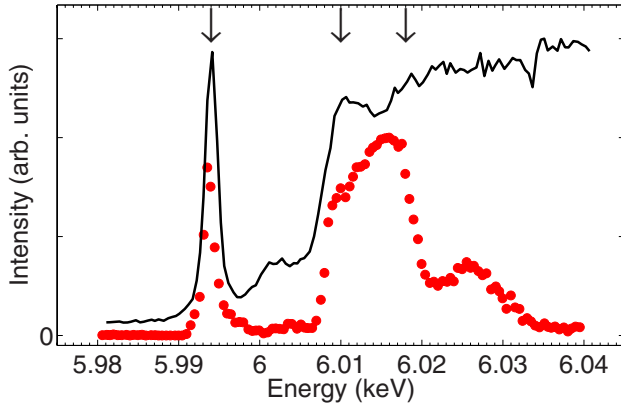
FIG. 3. (Color online) Experimental data on fluorescence yield (black solid line) and energy scan (red symbols) for the (130) reflection in the $\pi \rightarrow \sigma'$ polarization configuration. Arrows indicate the energy values where Stokes' parameters were measured.
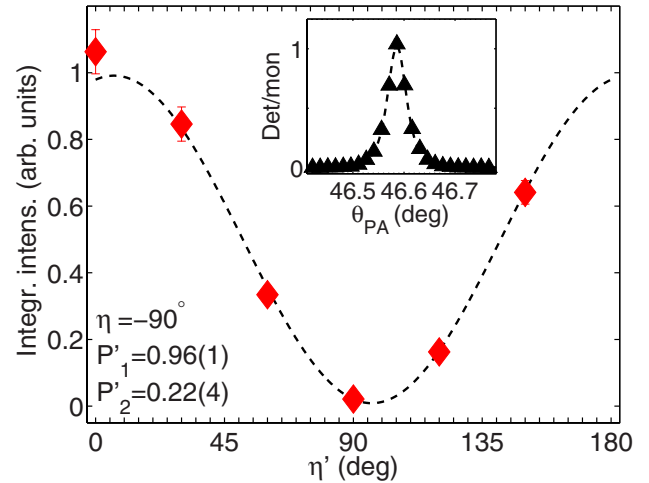

FIG. 4. (Color online) Variation of the integrated intensity of the (130) forbidden Bragg peak as a function of the polarization analyzer angle η'. The dashed line represents a fit to these data with Eq. (3) (see text for details). The inset is an example of a rocking scan of the analyzer: the integrated intensity obtained from the fit (dashed line: Lorentzian squared and linear background) represents experimental point in the main axes.

a cryostat was used to stabilize the temperature at 300 K. Sample rocking curves (θ scans) of the crystal resulted in widths smaller than 0.01°, indicating a high sample quality.

A diamond phase plate of thickness 700 μm with a [110] surface was inserted into the incident beam, within its own goniometer, and the (111) Bragg reflection in symmetric Laue geometry was selected to modify the polarization of the x-ray beam incident on the diffractometer. The phase plate was operated in either quarter-wave or half-wave plate mode. With the former we generated left-or right-circular polarization $P_3 \approx \pm 1$, whereas with the latter we rotated the linear incident polarization into an arbitrary plane,[25,26] described by $P_1 \approx \cos(2\eta)$ and $P_2 \approx \sin(2\eta)$. Here η is the angle between the incident beam electric field vector and the vertical axis (see Fig. 2)—i.e., $\eta = 0$ when the polarization is perpendicular to the horizontal scattering plane (σ polarization).

The sample was mounted with the [010] and [100] directions defining the horizontal scattering plane. Figure 3 shows the fluorescence yield and the energy dependence of the glide-plane forbidden (130) reflection, collected at an azimuthal angle of $\Psi = -0.78(3)°$ degrees with respect to the reciprocal lattice direction [010]. The photon energy was then tuned to the pre-edge region of the Cr K edge (5994 eV). An x-ray polarization analyzer was placed in the scattered beam. It exploited the (220) Bragg reflection of a LiF crystal, scattering close to a Brewster's angle of 45°. The polarization analyzer setup was rotated around the scattered beam by an angle η', and at each point the integrated intensity was determined by rocking the analyzer's theta axis (θ_{PA}). An example is shown in the inset of Fig. 4. The resulting integrated intensities were then fitted to the equation

$$I = \frac{P_0'}{2}[1 + P_1' \cos 2\eta' + P_2' \sin 2\eta'], \qquad (3)$$

to obtain the Poincaré-Stokes parameters P_1' and P_2'. An example is shown in Fig. 4 for $\eta = -90°$. The degree of circular polarization, P_3', cannot be measured directly in this setup. However, an upper limit is inferred from $P_1'^2 + P_2'^2 + P_3'^2 \lesssim 1$

(the equality holding for a completely polarized beam).

We systematically measured P_1' and P_2' of the beam scattered at the (130) reciprocal lattice point as function of η. Figure 5 shows both the experimental data (symbols) and the theoretical calculation (dashed lines), described below. The measured degree of linear polarization of the scattered beam, $P_1'^2 + P_2'^2$, strongly deviates from 100% in the range $-10° \lesssim \eta \lesssim 50°$, indicating that a large component of the scattered beam is either circularly polarized or depolarized. To ascertain which of these two processes is realized we reconfigured the diamond phase plate to produce circularly polarized x rays. Figure 6 shows the measured P_1' and P_2' for both linearly and circularly polarized x rays. The presence of linearly scattered x rays for the circular incident case is consistent with the assumption that the region for which $P_1'^2 + P_2'^2$ strongly deviates from 1 corresponds to an increased circularly polarized contribution. Furthermore, the calculations for $P_3'^2$, detailed in Sec. III, involving only completely polarized contributions to the scattered beam, agree well with its upper limit inferred from the data ($P_3'^2 \equiv 1 - P_1'^2 - P_2'^2$), indicating that the signal is essentially circularly polarized.

III. THEORETICAL DISCUSSION

In RXS the global process of photon absorption, virtual photoelectron excitation, and photon re-emission is coherent throughout the crystal, thus giving rise to the usual Bragg diffraction condition $\sum_j e^{i\mathbf{Q}\cdot\mathbf{R}_j}(f_{0j} + f_j' + if_j'')$. Here $\mathbf{R}_j$ stands for the position of the scattering center j, $\mathbf{Q}$ is the diffraction vector, and f_{0j} is the Thomson factor. f_j' and f_j'', related by the Kramers-Kronig transform, are given, at resonance, by the expression[1]
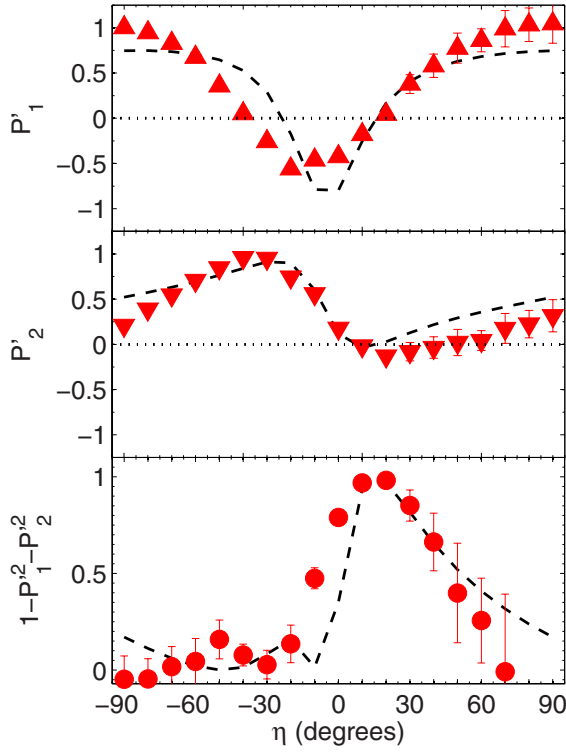
FIG. 5. (Color online) Calculated (dashed lines) and measured (symbols) Stokes' parameters for (130) reflection versus the polarization angle of the linear incoming light (see Fig. 2), E = 5.994 keV. See text for details.

$$f_j' + if_j'' \equiv f_j(\omega) \propto - \omega^2 \sum_n \frac{\langle \psi_g(j)|\hat{O}'^*|\psi_n\rangle\langle\psi_n|\hat{O}|\psi_g(j)\rangle}{\omega - (\omega_n - \omega_g) - i\frac{\Gamma_n}{2}},$$

$$(4)$$

where ω is the photon energy, ω_g is the ground-state energy, ω_n and Γ_n are the energy and inverse lifetime of the excited states, $\psi_g(j)$ is the core ground state centered around the jth atom, ψ_n is the photoexcited state, ϵ and ϵ' are the polarizations of the incoming and outgoing photons, and **q** and **q**′ are their corresponding wave vectors. The sum is extended over all excited states of the system. The transition operator $\hat{O}^{(\prime)}$ = $\boldsymbol{\epsilon}^{(\prime)}\cdot\mathbf{r}(1-\frac{i}{2}\mathbf{q}^{(\prime)}\cdot\mathbf{r})$ is written as a multipolar expansion of the photon field up to electric dipole ($E1$) and quadrupole ($E2$) terms; **r** is the electron position relative to the resonating ion, $\boldsymbol{\epsilon}^{(\prime)}$ is the polarization of the incoming (outgoing) photon, and $\mathbf{q}^{(\prime)}$ is its corresponding wave vector.

By taking into account the space group symmetry of K$_2$CrO$_4$ (*Pnma*, No. 62), the four equivalent Cr sites at Wyckoff 4c positions (with local mirror-plane $\hat{m}_y$) can be related to one another by the following symmetry operations: $f_3 = \hat{I}f_1$, $f_4 = \hat{C}_{2x}f_1$, and $f_2 = \hat{I}f_4$. $\hat{I}$ is the space-inversion operator, and $\hat{C}_{2x}$ is the π-rotation operator the x axis. The Thomson scattering f_{0j} does not contribute at (1k0)-type reflections, for any k, due to the glide plane extinction rule. Therefore, the structure factor at the Cr K edge for the (1k0) chosen
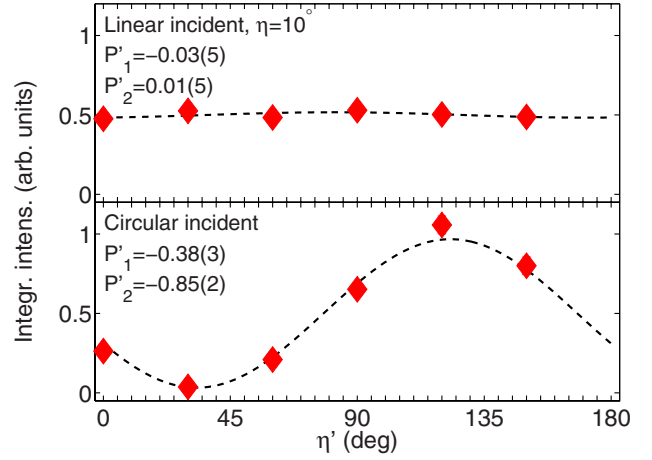

FIG. 6. (Color online) Stokes' parameters for (130) reflection with (top) linearly (η=10°) and (bottom) circularly polarized incident x rays, collected at E=5.994 keV. Dashed lines are fit with Eq. (3).

reflections, when summed over all equivalent sites, becomes, for $E1$-$E2$ scattering,

$$S = 2i \sin\left[2\pi\left(x + \frac{k}{4}\right)\right](1 - \hat{m}_z)f_1, \qquad (5)$$

while for $E1$-$E1$ and $E2$-$E2$ scattering it is given by

$$S = 2 \cos\left[2\pi\left(x + \frac{k}{4}\right)\right](1 - \hat{m}_z)f_1. \qquad (6)$$

Here $x \simeq 0.23$ is the fractional coordinate of Cr atoms and $\hat{m}_z$ is a glide-plane orthogonal to the z axis. In deriving Eqs. (5) and (6), we have used the identity $f_1 = \hat{m}_y f_1$. It is interesting to note the different behavior of the two terms for k even or odd. For example, when k=4, the $E1$-$E2$ scattering is proportional to $\sin(2\pi x) \simeq 0.99$ and it dominates the other terms proportional to $\cos(2\pi x) \simeq 0.12$. Indeed we found the presence of a very intense pre-edge feature from the $E1$-$E2$ channel at the (140) reflection that is related to the electric octupole moment, as predicted in Ref. 27 and verified numerically by our *ab initio* calculations. However, as described above, the presence of a single-scattering channel, as in the case of the (140) reflection, cannot lead to a circularly polarized diffracted beam. This can be demonstrated by a symmetry argument: if only one scatterer is present, which is by hypothesis nonmagnetic, and the incident light is linearly polarized, then the initial state is time reversal even. Therefore, as matter-radiation interaction does not break time-reversal, it follows that the final state must also be time-reversal even; i.e., radiation can not be circularly polarized, which would break time reversal. This is no more true when two scatterers are present, due to the extra degree of freedom represented by the time (phase) delay between the two scattering processes. Indeed, this was *a posteriori* verified by our numerical simulation, which confirmed that no outgoing circular polarization is present at the (140) reflection.

The case of the (130) reflection is very different. The role of $\sin(2\pi x)$ and $\cos(2\pi x)$ in Eqs. (5) and (6) switches in

such a way that the two diffraction channels $E1$-$E1$ and $E2$-$E2$ become predominant. Further analysis of the structure factor[28] reveals that two resonances are allowed, one for each channel, corresponding to an electric quadrupole ordering for the $E1$-$E1$ scattering and an electric hexadecapole[19] for the $E2$-$E2$ scattering. Finally, multiple-scattering calculations with the FDMNES program confirm that the two resonances overlap in the pre-edge region, though slightly shifted in energy of ~ 1 eV. These are the conditions to be met to get the interference of the two channels. In order to describe the effect quantitatively from a theoretical point of view we used the *ab initio* code FDMNES, in the multiple-scattering mode, to calculate P_3 directly from Eq. (4) for the K_2CrO_4 structure.[21] We employed a cluster of 43 atoms, corresponding to a radius of 5.5 Å around the resonating Cr-atom. Notice that in this most general case we find $P'_3(\omega) \propto f'_{E1}(\omega) f''_{E2}(\omega) - f'_{E2}(\omega) f''_{E1}(\omega)$ where f' and f'' are the usual dispersive and absorptive terms [see Eq. (4)] for $E1$ and $E2$ channels. Therefore, at the photon energy ω, P'_3 is determined by the interference of the absorptive part f'' of one channel with the dispersive part f' of the other and, again, in the presence of just one channel, $P'_3=0$.

The numerical simulations shown in Fig. 5 (dashed lines) confirm that there is an azimuthal region where the incoming linear polarization is fully converted into an outgoing circular polarization and that the effect is determined by the interference of the $E1$-$E1$ and $E2$-$E2$ channels.

In this respect, it is interesting to note that the origin of this effect is profoundly different from those determined by a chiral (magnetic) structure (see, e.g., Refs. [29,30]), as clearly seen by the fact that all the tensors involved are nonmagnetic and parity even.

Finally, we verified experimentally that at the Cr K edge ($E=6010$ and 6018 eV), where only one term in the $E1$-$E1$ channel is present, no circular polarization was observed for all incident angles—i.e., $P'^2_1+P'^2_2=1$. Calculations performed using FDMNES confirmed this result.

IV. CONCLUSIONS

Polarization analysis of RXS experiments has developed greatly in the last few years, helping to understand several characteristics of order parameters in transition-metal oxides, rare-earth-based compounds, and actinides. Up to now, however, the full investigation of Stokes' parameters was not applied most likely because linear polarization analysis, where only the P'_1 parameter was determined by measuring the $\sigma \rightarrow \sigma'$ and $\sigma \rightarrow \pi'$ channels, was considered sufficient. While this may be true when just one excitation channel is involved [as at the (140) reflection in the present case], several dephasing phenomena may appear when two different multipole excitations close in energy are involved in the transition. As we have seen, these phenomena may lead to a situation where incoming linear polarization is scattered to a circular polarization due to an interference between two multipoles, at the same time allowing for a very sensitive determination of the presence of the second multipole. We believe that the use of phase plates and of a complete polarization analysis is the key to disentangle multiresonance structures in those situations where an usual energy scan, like the one shown in Fig. 3, is not sufficient to this aim. The effect of d-band filling on details of the electronic structure will be investigated by the method presented here in the series of isostructural compounds $K_2CrO_4 \rightarrow K_2MnO_4 \rightarrow K_2FeO_4$.

[1] M. Blume, in *Resonant Anomalous X-ray Scattering*, edited by G. Materlik, C. J. Sparks, and K. Fischer (Elsevier Science, Amsterdam, 1994), p. 495.

[2] Y. Murakami, H. Kawada, H. Kawata, M. Tanaka, T. Arima, Y. Moritomo, and Y. Tokura, Phys. Rev. Lett. **80**, 1932 (1998).

[3] Y. Murakami, J. P. Hill, D. Gibbs, M. Blume, I. Koyama, M. Tanaka, H. Kawata, T. Arima, Y. Tokura, K. Hirota, and Y. Endoh, Phys. Rev. Lett. **81**, 582 (1998).

[4] Y. Joly, S. Grenier, and J. E. Lorenzo, Phys. Rev. B **68**, 104412 (2003).

[5] S. B. Wilkins, P. D. Hatton, M. D. Roper, D. Prabhakaran, and A. T. Boothroyd, Phys. Rev. Lett. **90**, 187201 (2003).

[6] S. B. Wilkins, P. D. Spencer, P. D. Hatton, S. P. Collins, M. D. Roper, D. Prabhakaran, and A. T. Boothroyd, Phys. Rev. Lett. **91**, 167205 (2003).

[7] M. Kubota, T. Arima, Y. Kaneko, J. P. He, X. Z. Yu, and Y. Tokura, Phys. Rev. Lett. **92**, 137401 (2004).

[8] J. Goulon, C. Goulon-Ginet, A. Rogalev, V. Gotte, C. Malgrange, C. Brouder, and C. R. Natoli, J. Chem. Phys. **108**, 6394 (1998).

[9] S. Di Matteo, Y. Joly, and C. R. Natoli, Phys. Rev. B **72**, 144406 (2005).

[10] J. A. Paixão, C. Detlefs, M. J. Longfield, R. Caciuffo, P. Santini, N. Bernhoeft, J. Rebizant, and G. H. Lander, Phys. Rev. Lett. **89**, 187202 (2002).

[11] S. Di Matteo, Y. Joly, A. Bombardi, L. Paolasini, F. de Bergevin, and C. R. Natoli, Phys. Rev. Lett. **91**, 257402 (2003).

[12] T. H. Arima, J. H. Jung, M. Matsubara, M. Kubota, J. P. He, Y. Kaneko, and Y. Tokura, J. Phys. Soc. Jpn. **74**, 1419 (2005).

[13] R. Caciuffo, J. A. Paixão, C. Detlefs, M. J. Longfield, P. Santini, N. Bernhoeft, J. Rebizant, and G. H. Lander, J. Phys.: Condens. Matter **15**, S2287 (2003).

[14] C. M. Varma, Phys. Rev. B **55**, 14554 (1997).

[15] C. M. Varma, Phys. Rev. Lett. **83**, 3538 (1999).

[16] D. Mannix, G. H. Lander, J. Rebizant, R. Caciuffo, N. Bernhoeft, E. Lidström, and C. Vettier, Phys. Rev. B **60**, 15187 (1999).

[17] L. Paolasini, C. Vettier, F. de Bergevin, F. Yakhou, D. Mannix, A.

Stunault, W. Neubeck, M. Altarelli, M. Fabrizio, P. A. Metcalf, and J. M. Honig, Phys. Rev. Lett. **82**, 4719 (1999).

[18] K. D. Finkelstein, Q. Shen, and S. Shastri, Phys. Rev. Lett. **69**, 1612 (1992).

[19] P. Carra and B. T. Thole, Rev. Mod. Phys. **66**, 1509 (1994).

[20] L. Paolasini *et al.* (unpublished).

[21] D. H. Templeton and L. K. Templeton, Phys. Rev. B **49**, 14850 (1994).

[22] L. Paolasini, C. Detlefs, C. Mazzoli, S. B. Wilkins, P. P. Deen, A. Bombardi, N. Kernavanois, F. de Bergevin, F. Yakhou, J.-P. Valade *et al.*, J. Synchrotron Radiat. **14**, 301 (2007).

[23] M. Blume and D. Gibbs, Phys. Rev. B **37**, 1779 (1988); M. Born and E. Wolf, in *Principles of Optics* (Cambridge University Press, Cambridge, England, 1999); R. C. Jones, J. Opt. Soc. Am. **31**, 448 (1941); **31**, 500 (1941).

[24] Y. Joly, Phys. Rev. B **63**, 125120 (2001); the program can be freely downloaded at the web address http://www-cristallo.grenoble.cnrs.fr/fdmnes

[25] C. Giles, C. Vettier, F. de Bergevin, C. Malgrange, G. Grübel, and F. Grossi, Rev. Sci. Instrum. **66**, 1518 (1995).

[26] L. Bouchenoire, S. D. Brown, P. Thompson, C. Detlefs, and M. J. Cooper, Nucl. Instrum. Methods Phys. Res. A **566**, 733 (2006).

[27] I. Marri and P. Carra, Phys. Rev. B **69**, 113101 (2004).

[28] The application of the structure-factor symmetry operation $\hat{m}_z$ on the irreducible tensor representing the atomic scattering factor (Ref. [11]) leads to $\hat{m}_z f_q^{(r)} = (-)^{(q+P)} f_q^{(r)}$, where p is the parity of the tensor (+1 for E1-E1 and E2-E2, −1 for E1-E2). From this rule the allowed multipole components follow.

[29] C. Sutter, G. Grübel, C. Vettier, F. de Bergevin, A. Stunault, D. Gibbs, and C. Giles, Phys. Rev. B **55**, 954 (1997).

[30] J. C. Lang, D. R. Lee, D. Haskel, and G. Srajer, J. Appl. Phys. **95**, 6537 (2004).